

Microstructure and Properties of Fe–Cr–B–Al Alloy After Heat Treatment

Cheng Xiao-le¹ · Ju Jiang² · Qu Yin-hu¹ · Cao Li² · Fu Han-guang¹

Received: 14 January 2018 / Accepted: 5 June 2018 / Published online: 29 June 2018
© The Indian Institute of Metals - IIM 2018

Abstract By means of optical microscope, scanning electron microscope, X-ray diffraction, energy dispersive spectrometer, Rockwell and Vickers hardness tester, and wear tester, the microstructure and properties of Fe–10Cr–1B–4Al alloy quenched in different temperature has been studied. The results show that the microstructure of as-cast Fe–10Cr–1B–4Al are composed of pearlite, ferrite and the eutectic borocarbide which shows a network distribution along grain boundaries. The eutectic borocarbides are composed of $M_7(C, B)_3$, $M_2(B, C)$ and $M_{23}(C, B)_6$. As the quenching temperature increases, the network structure of eutectic borocarbide breaks, but the type of eutectic borocarbide has no obvious change, and the matrix structure changes gradually from ferrite to pearlite. As the quenching temperature increases, the macro-hardness and the matrix micro-hardness of Fe–10Cr–1B–4Al alloy increases gradually. The macro-hardness and matrix micro-hardness of alloy reach the highest value of 45.7 HRC and 388.1 HV, respectively when the quenching temperature is 1150 °C. The hardness of alloy decreases slightly when the quenching temperature is too high. While quenching at 1150 °C, the alloy has the highest wear resistance and good comprehensive properties.

Keywords Fe–Cr–B–Al alloy · Quenching temperature · Microstructure · Hardness · Wear resistance

1 Introduction

Wear is one of the most important causes of equipment failure and material failure in industry, and it is also one of the most serious economic losses [1]. Many scholars at home and abroad pay great attention in developing new type wear-resistant materials and reducing wear and tear. High chromium white cast iron has excellent performance. However, it contains Mo, Ni and other expensive alloy elements, which greatly improves the cost of the alloy [2–4]. The solubility of B element in the α -Fe is less than 0.0004 wt%. The solubility of B element in the γ -Fe is 0.02 wt%. Moreover, the atomic radius of boron atom is larger than that of carbon atom, so the excess boron elements will form the hard phase [5, 6].

Presently high boron wear-resistance alloy has been developed at home and abroad [7, 8]. In order to improve the hardenability of the high boron wear-resistant alloy, reduction of the brittle boride phase is necessary. The Fe–Cr–B alloy is obtained by adding Cr element into the Fe–B alloy [9, 10]. The performance of Fe–Cr–B alloy is obviously superior to that of Fe–B alloy. Some studies [11, 12] found that while adding the aluminum element in the Fe–B alloy, only a small amount of aluminum element is dissolved in the boride. Excess aluminum elements excreted during the formation and growth of boride inhibit the formation of the boride network. Aluminum can also improve the strength, hardness and oxidation resistance of the alloy.

In this paper, a new type of Fe–Cr–B–Al alloy has been proposed, and the influence of heat treatment process on

✉ Fu Han-guang
fhg64@263.net

¹ School of Mechanical and Electrical Engineering, Xi'an Polytechnic University, Jinhua Road No. 19, Beilin District, Xi'an 710048, Shaanxi Province, People's Republic of China

² School of Materials Science and Engineering, Beijing University of Technology, Beijing 100124, People's Republic of China

the microstructure and properties of Fe–Cr–B–Al alloy has been studied. It is expected to provide the reference for the industrial application of this newly proposed material.

2 Experimental Procedure

2.1 Materials and Specimens

The experimental material was smelted with a vacuum induction melting furnace of 10 kg. The raw materials were scrap steel, pure aluminum, Fe–20wt%B, Fe–62wt% Cr, Fe–75wt% Si and Fe–78wt% Mn. At the same time, an appropriate amount of carbon additive was added. The design composition of Fe–10Cr–1B–4Al alloy is shown in Table 1. In the smelting process, when the temperature of molten steel rose to 1530–1550 °C, pure aluminum was inserted, then the molten steel was subsequently superheated to 1650 °C and transferred into a preheated teapot ladle. After removal of any dross and slag, the melt was poured at 1500 °C into the metal molds to produce ingots of \varnothing 80 mm \times 200 mm, followed by air cooling to room temperature. XRF was used to determine the chemical composition of as-cast specimens. The actual composition of the Fe–10Cr–1B–4Al alloy is shown in Table 2. The results showed that the actual chemical composition of the alloy is basically the same as the design and meets the test requirements. All samples for analysis were obtained from the center of the ingots by wire-cutting [13].

2.2 Microstructure Analysis

Figure 1 represents the vertical sections of Fe–10Cr–1B–4Al alloy. It could be observed that the austenitizing temperature of the test alloy was about 1000–1300 °C. To avoid excessive burning and severe oxidation of the specimens, the quenching temperature was controlled below 1300 °C. So the specimens were heat-treated at 1000, 1030, 1060, 1090, 1120, 1150 and 1180 °C for 1 h,

Table 1 The designed chemical composition of Fe–10Cr–1B–4Al alloy (wt%)

Cr	Al	B	C	Si	Mn	Ni	Fe
10.0	4.0	1.0	0.3	0.7	0.8	0.1	Bal.

Table 2 Actual chemical composition of Fe–10Cr–1B–4Al alloy determined by XRF (wt%)

Cr	Al	B	C	Si	Mn	Ni	Fe
9.47	4.21	0.99	0.30	0.79	0.85	0.11	Bal.

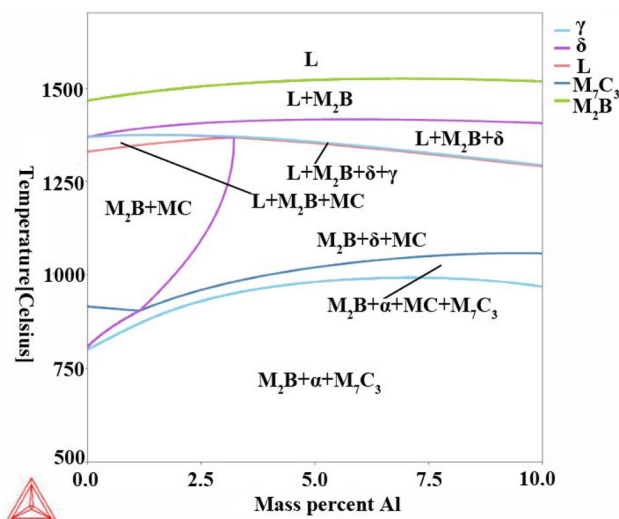


Fig. 1 Vertical sections of Fe–10Cr–1B–Al quinary system [14]

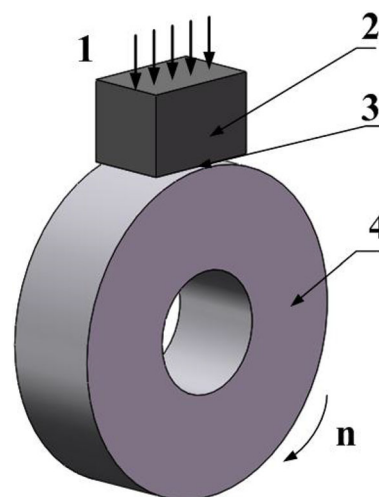


Fig. 2 Schematic of block-on-ring wear testing machine [15–17]: 1—load; 2—specimen; 3—ring-block contact surface; 4—grinding ring; n—rotation rate

respectively, and quenched in the water. The heat treatment was carried out in the chamber electric furnace. In order to prevent the specimens from oxidizing seriously during the heating process, the surface of the specimens was coated with anti-oxidation paint.

The specimens were ground with 240#, 400#, 600#, 800#, 1000#, 1500#, and 2000# sandpaper. After polishing, alcohol washing and drying, the samples were etched with 4% CuSO₄ solution, washed with alcohol, and blow-dried. The microstructure and phase distribution of the alloys were analyzed using an OLYMPUS BX-51 optical microscope and a Japanese Hitachi S-3400 scanning electron microscope with energy dispersive spectrometer. X-ray diffraction was performed on a SHIMADZU Japan

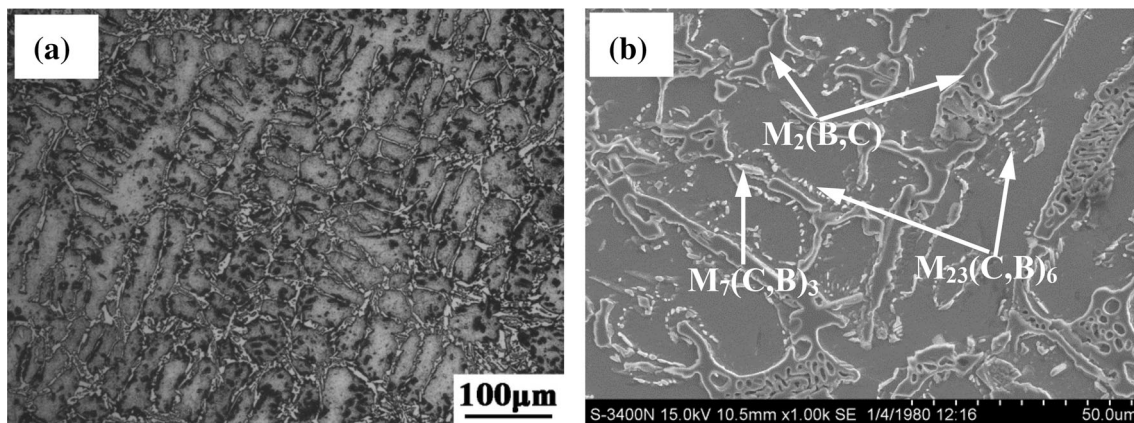


Fig. 3 Metallographic (a) and scanning (b) photos of as-cast Fe-10Cr-1B-4Al alloy

XRD-7000 diffractometer with copper $K\alpha$ radiation coupling continuous scanning at 40 kV and 200 mA as an X-ray source. The specimen was scanned with the angle 2θ ranging from 10° to 90° with a step size of 0.2° and a collection time of 10 s.

2.3 Mechanical Properties and Wear Resistance Test

The macro-hardness measurement was done using an HR-150A-type Rockwell hardness tester. The test load was 1470 N. The micro-hardness of the matrix was measured by means of an HV-1000 digital display micro Vivtorinox hardness tester with a load of 1.96 N and the time of 12 s. Five indentations were made on each sample under each experimental condition to check reproducibility of the hardness data.

The wear test was conducted on a MM-2000 ring block abrasion tester, as shown in Fig. 2 [15–17]. The sample size was $10\text{ mm} \times 10\text{ mm} \times 15\text{ mm}$. GCr15 grinding rings were used, with a hardness of 60–62 HRC, a size of $\phi 40\text{ mm} \times 10\text{ mm}$. The chemical compositions of GCr15 grinding rings were 1.03wt%C, 1.49wt%Cr, 0.35wt%Mn and 0.27wt%Si [18]. The test load was 588 N, the test temperature was 20°C , the wear time was 30 min, and the rotation rate of tester wheel was 200 rpm. Three samples were taken from each group to measure the difference in mass before and after wear. The average weight loss of the three samples was used as the final wear. The balance was measured with a TG328B, and the weighing range was 200 g, with a quantity of 0.1 mg. The worn surface was observed using a JSM6510 electron microscope with an energy dispersive spectrometer.

3 Results and Discussion

3.1 Microstructure of Fe-10Cr-1B-4Al Alloy

The microstructures and XRD pattern of Fe-10Cr-1B-4Al alloy in the as-cast condition are shown in Figs. 3 and 4. The tested alloy is composed of matrix and hard phase. The matrix is identified as α -Fe solid solution (JCPDS 34-0396). The lattice constant (a) of α -Fe calculated by Prague formula is 0.2877 nm, which is greater than the normal lattice parameter of α -Fe (0.2866 nm), showing that the α -Fe of the tested alloy is supersaturated with alloying elements (mainly consists of C, Cr and Al). In addition, the matrix presents typical ferrite and pearlite morphology under OM (Fig. 3a).

In case of the hard phase in the sample, it is mainly composed of $M_2(B, C)$ -type borocarbide (M represents Cr, Fe, Mn, etc., JCPDS 36-1332), presenting fish-bone structures distributing around the matrix (as shown in

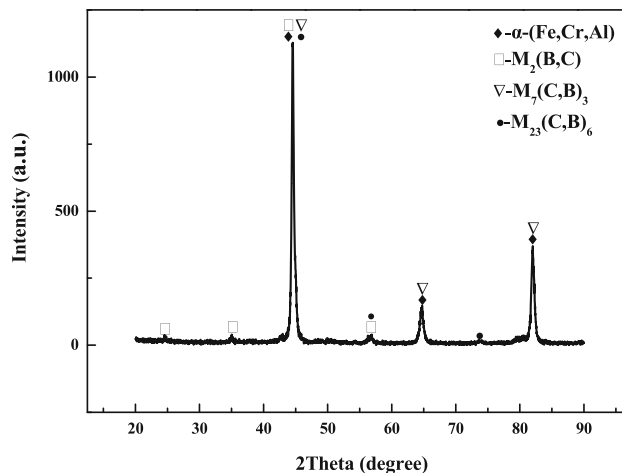


Fig. 4 The X-ray diffraction pattern of as-cast Fe-10Cr-1B-4Al alloy

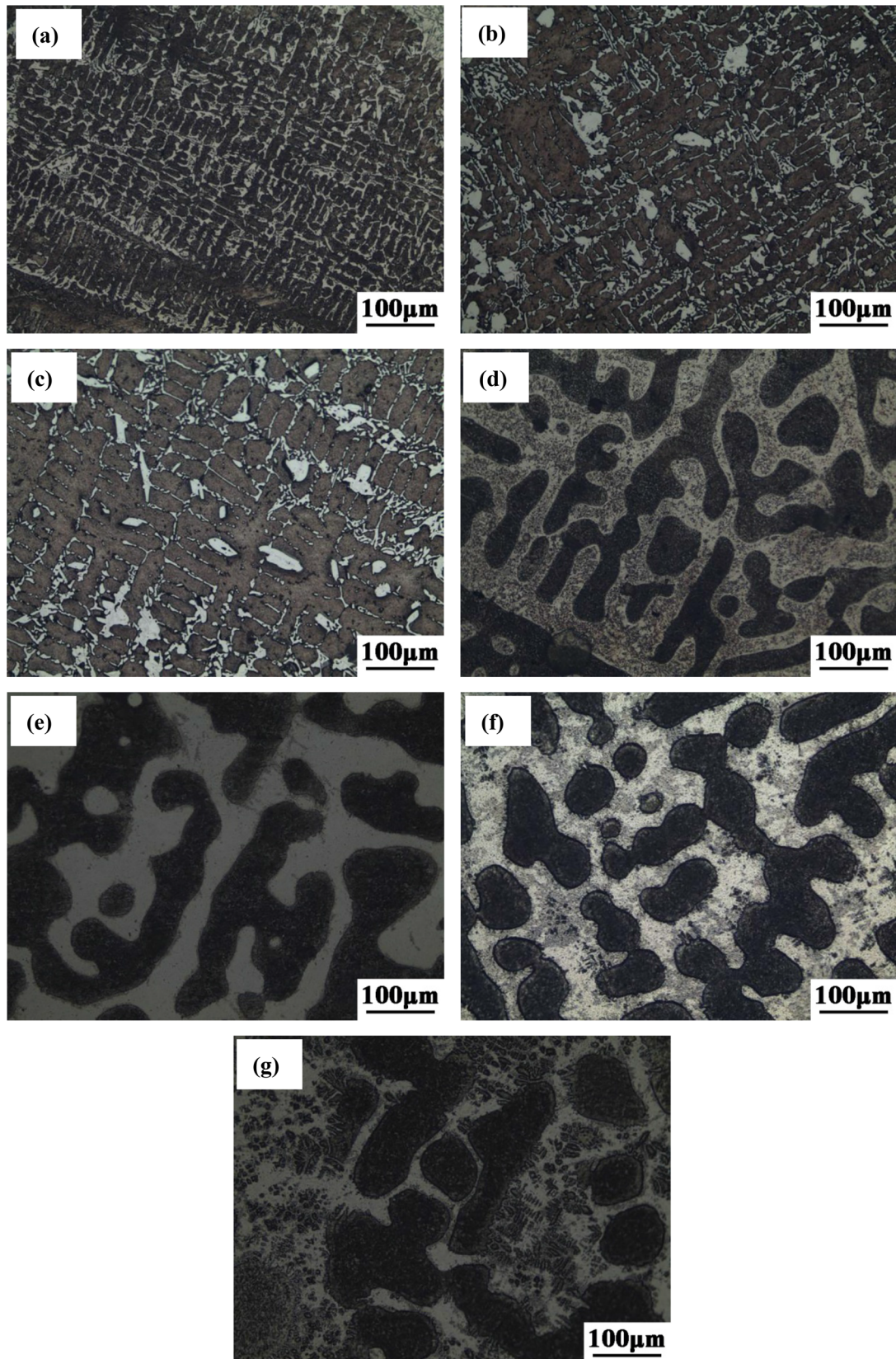


Fig. 5 Metallographic photos of Fe-10Cr-1B-4Al alloy after quenching: **a** 1000 °C, **b** 1030 °C, **c** 1060 °C, **d** 1090 °C, **e** 1120 °C, **f** 1150 °C, **g** 1180 °C

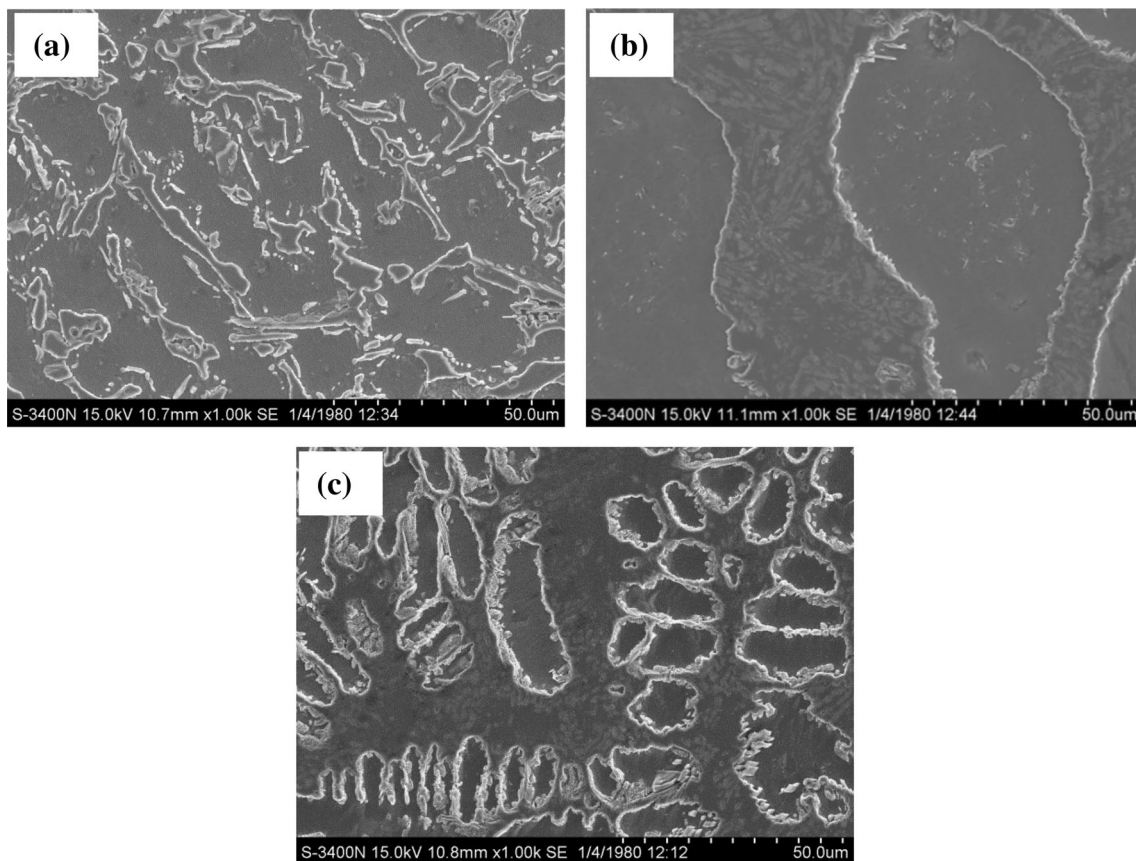


Fig. 6 SEM pictures of Fe-10Cr-1B-4Al alloy after quenching: **a** 1000 °C, **b** 1150 °C, **c** 1180 °C

Fig. 3b). In addition, there are a small amount of $M_7(C, B)_3$ and $M_{23}(C, B)_6$ -type borocarbide (M represents Cr, Fe, Mn, etc., JCPDS 47-1332 and JCPDS 35-1180) in the hard phase. As shown by the arrows in Fig. 3b, the $M_2(B, C)$ is mainly fish-bone, the $M_7(C, B)_3$ is mainly central reticular and the $M_{23}(C, B)_6$ is mainly isolated nubbin. Due to the relatively high Cr/C ratio in the experiment examples, it is easy to form Cr_7C_3 during the solidification. But the solubility of boron in the γ -Fe is very low, only 0.02%. When the excess boron is added into the alloy, a portion of boron forms M_2B at the grain boundary through segregation, another part of boron dissolves into Cr_7C_3 to form $Cr_7(C, B)_3$ [19]. At the same time, since the atomic arrangements of Fe_7C_3 and Cr_7C_3 are similar, and the atomic sizes of chromium and iron are similar, a large number of Cr atoms substitute Fe atoms, thus forming $M_7(C, B)_3$. Moreover, the Cr element can reduce the chemical potential of C in Fe, contributing to the formation of a stable compound [20].

Figures 5 and 6 represent respectively the optical micrograph and SEM pictures of Fe-10Cr-1B-4Al alloy after quenching with different temperature. Figure 7 shows the X-ray diffraction spectrums of Fe-10Cr-1B-4Al alloy after quenching with different temperature. It can be seen that the network structure of eutectic structure begin to

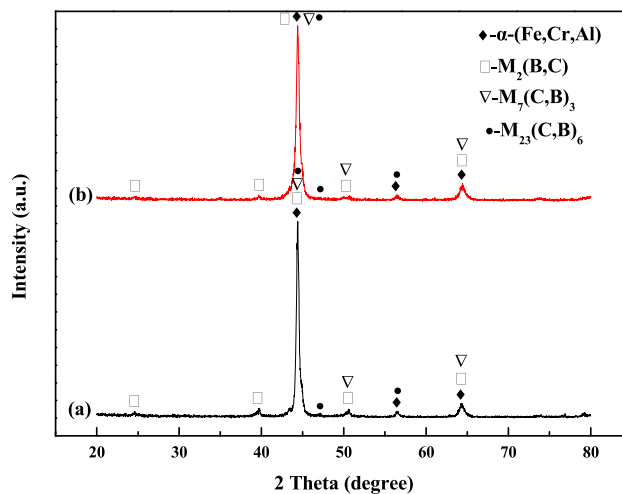


Fig. 7 The X-ray diffraction pattern of Fe-10Cr-1B-4Al alloy after quenching with different temperature: **a** 1000 °C and **b** 1150 °C

break after 1000 °C quenching treatment, and the eutectic carbide disperse in the matrix. It also can be seen that the number of ferrite in matrix decreases gradually, and the quantity of pearlite increases gradually. But the quenching treatment does not change the type of hard phase. From Figs. 5b–g, as the quenching temperature increases, the

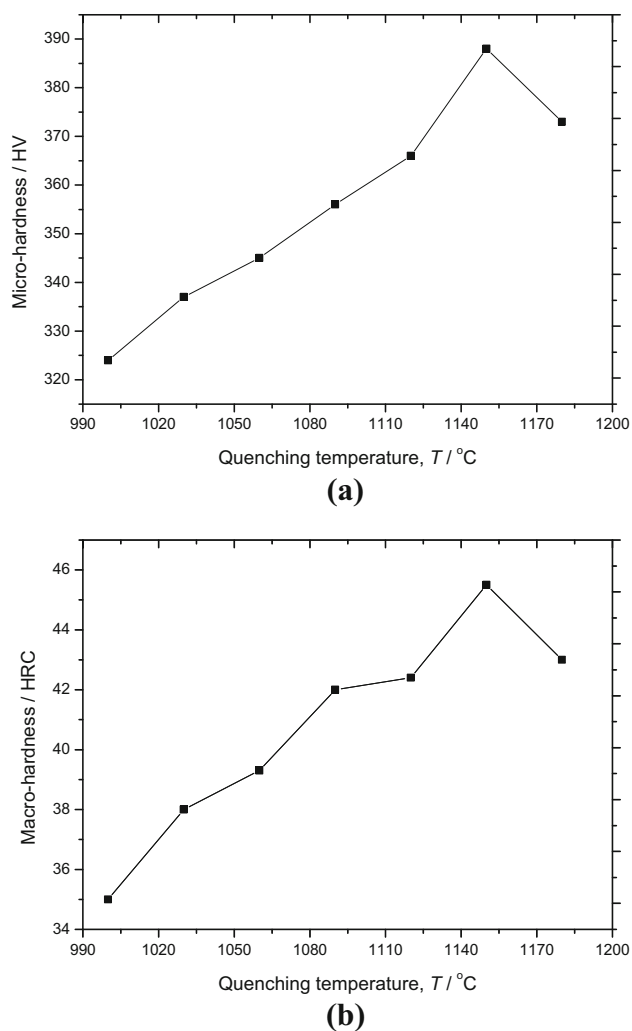


Fig. 8 Effect of quenching temperature on matrix micro-hardness (a) and macro-hardness (b) of Fe-10Cr-1B-4Al alloy

microstructure of matrix of Fe-10Cr-1B-4Al alloy is completely transformed into pearlite. The trend of fracture of eutectic structure is more and more obvious. The amount of granular precipitates in matrix decreases gradually. When the quenching temperature reaches 1150 °C, the breaking effect of eutectic structure is ideal and the microstructure is small, which is beneficial to improve the comprehensive properties of Fe-10Cr-1B-4Al alloy.

However, as the quenching temperature continues to rise, the eutectic microstructure tends to become coarse, and Fig. 6c shows that the particulate precipitates almost disappear. When the quenching temperature is more than 1090 °C, the network structure of eutectic borocarbide will be completely disconnected, into small strips. And this eutectic borocarbide will diffuse along the grain boundaries and form a new structure resembling a mesh. Boron and carbon atoms diffuse from higher degrees to lower degrees in the process of high temperature heat treatment, which

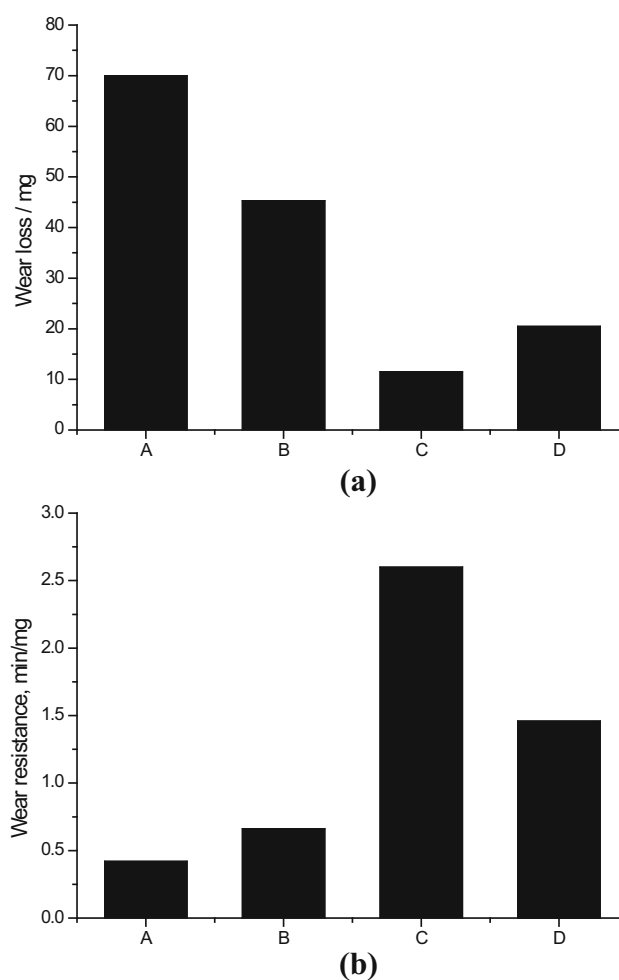


Fig. 9 Effect of quenching temperature on wear loss (a) and wear resistance (b) of Fe-10Cr-1B-4Al alloy. A: as-cast, B: quenching at 1000 °C, C: quenching at 1150 °C, D: quenching at 1180 °C

determines the dissolution of the network structure of boron carbide [12]. Borocarbide preferentially dissolves in sharp corners or thin weak areas. It can be seen from the microstructure of as-cast Fe-10Cr-1B-4Al alloy that the network structure of borocarbide has been broken after adding 4wt%Al in alloy, and a number of unstable necking conditions are formed. This provides a favorable primitive microstructure for accelerating the breaking of the network structure of eutectic carbides during heat treatment. The increase of temperature accelerate the diffusion between the elements, thus speeding up the fracture of the network structure of borocarbide.

3.2 Effect of Quenching on Hardness of Fe-10Cr-1B-4Al Alloy

The effects of quenching temperature on the macro-hardness and the matrix micro-hardness of Fe-10Cr-1B-4Al

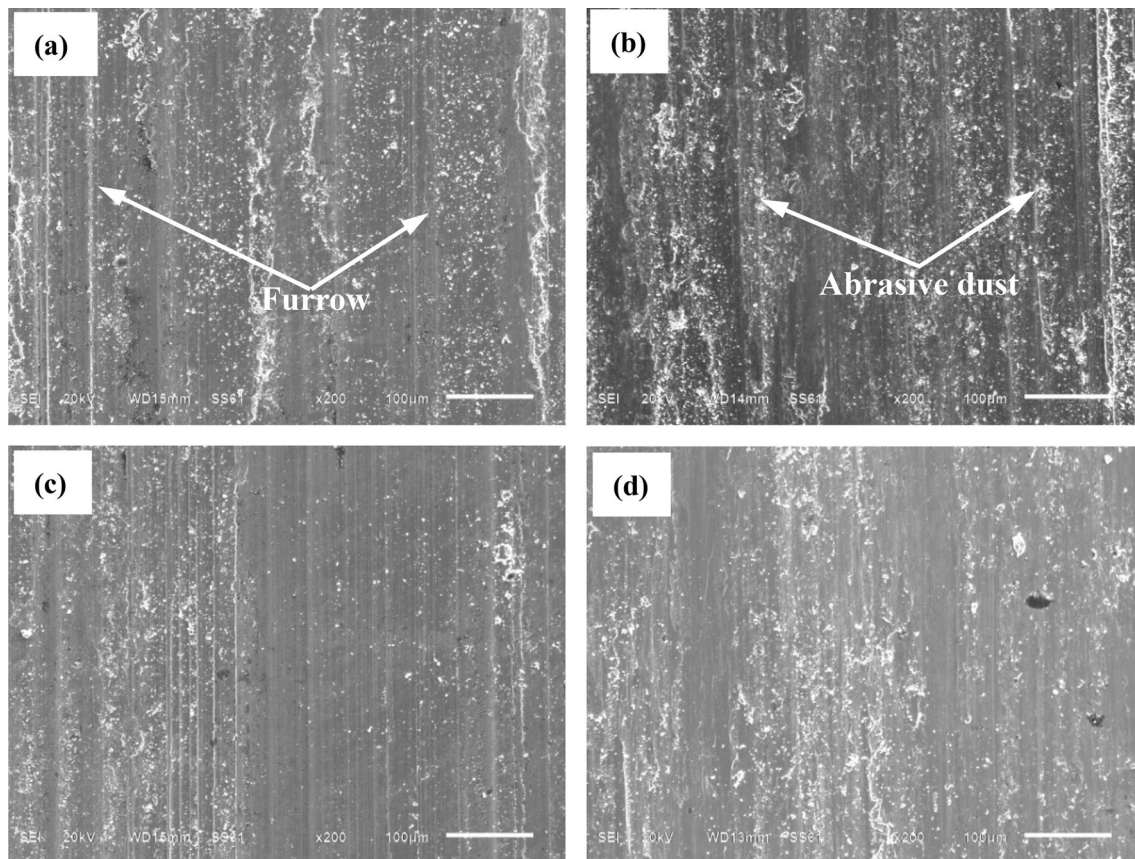


Fig. 10 The photos of worn surface of Fe–10Cr–1B–4Al alloy after quenching with different temperature: **a** as-cast; **b** 1000 °C; **c** 1150 °C; **d** 1180 °C

alloy are shown in Fig. 8. When the quenching temperature is lower than 1150 °C, the macro-hardness and the matrix micro-hardness of alloy increase gradually with the increase of quenching temperature. When the quenching temperature exceeds 1150 °C, the macro-hardness and the matrix micro-hardness of matrix have no obvious change. While quenching at 1150 °C, the macro-hardness and matrix micro-hardness of Fe–10Cr–1B–4Al alloy reach the highest value of 45.7 HRC and 388.1 HV, respectively. Because the ratio of water cooling is very fast, which make boron and aluminum atoms diffuse from intracrystalline to grain boundary. This makes supersaturated solid solution of boron and aluminum form in the matrix. Moreover, the literature [21] shows that the diameter ratio of boron and iron atoms is 0.7, which is significantly larger than the upper limit size of the interstitial solid solution of 0.59, and is significantly less than 0.86 of the formed substitutional solid solution. Therefore, in whatever manner the boron atoms are dissolved in the matrix, it will lead to large lattice distortion and improve the micro-hardness of the matrix. In addition, the results of microstructure analysis shows that as the quenching temperature increases, the network structure of eutectic borocarbide is obviously

broken and the microstructure is refined, which improves the bonding strength of intercrystalline. As a result of the combination, the macro-hardness of the alloy is slightly increased while quenching at 1150 °C. However, when the quenching temperature exceeds 1150 °C, more boron, carbon, aluminum and other alloy elements are dissolved in austenite, which greatly improves the stability of the austenite. At this time, there are more retained austenite in the structure after quenching, which results in a slight decrease in the hardness of the alloy.

3.3 Effect of Quenching on Wear Resistance of Fe–10Cr–1B–4Al Alloy

Figure 9 represents the effect of quenching on wear loss and wear resistance of the Fe–10Cr–1B–4Al alloy. It can be seen that when the quenching temperature is lower than 1150 °C, the wear-resistance of alloy increases gradually with the increasing of quenching temperature. However, the wear-resistance has a slight decrease when the quenching temperature exceeds 1150 °C. As the quenching temperature increases, the change law of wear loss of alloy is just opposite to that of the wear-resistance.

Because the hardness of the matrix of the as-cast alloy is low, the matrix with low hardness is first worn off at the initial stage of the wear, which makes the hard phase with high hardness become exposed. But in the process of the hard phase wear, the matrix with low hardness cannot protect the hard phase. This makes the hard phase fall off, and accelerates the cutting of the matrix. It will produce the debris and furrow in the process of wear, as shown in Fig. 10. The hardness of the alloy quenching at 1000 °C is still very low, so the wear effect is close to as-cast state. However, the hardness of the alloy is greatly improved after quenching at 1150 °C, the hardness of the matrix also is greatly improved. Then the matrix with high hardness will protect the hardness phase and prevent the hard phase from falling off. From Fig. 10c, the number of wear debris and furrows on the surface is greatly reduced. When the quenching temperature is too high, the hardness of the alloy decreases, and the wear-resistance of the alloy decreases slightly.

4 Conclusions

1. The microstructure of Fe–10Cr–1B–4Al alloy is mainly composed of ferrite, pearite and eutectic structure. The eutectic structure consists of $M_7(C,B)_3$, $M_2(B,C)$ and $M_{23}(C,B)_6$ type borocarbide.
2. After quenching, the matrix structure changes gradually from ferrite to pearlite. The type of eutectic borocarbide has no obvious change, but the network structure of eutectic borocarbide breaks.
3. When the quenching temperature is 1150 °C, the Fe–10Cr–1B–4Al alloy has the highest hardness and best wear-resistance, and its comprehensive properties are the best.

Acknowledgements The authors appreciate the financial support for this work from the Beijing Natural Science Foundation (2142009).

References

1. Röttger A, Weber S, and Theisen W, *Mater Sci Eng A* **532** (2012) 511521.
2. Filipovic M, Kamberovic Z, and Korac M, *Mater Trans* **52** (2011) 386.
3. Mohammadnezhad M, Javaheri V, Shamanian M, Naseri M, and Bahrami M, *Mater Design* **49** (2013) 888
4. Scandian C, Boher C, Mello J D B D, and Rézai-Aria F, *Wear* **267** (2009) 401
5. Gong J X, Li H, Xiao Y F, and Zhang Q H, *J Mater Eng* (2009) 22
6. Perrier M, Deschamps A, Bouaziz O, Brechet Y, Danoix F, Geuser FD, Donnadiou P, Hoummada K, and Maugis P, *Metall Mater Trans A* **43** (2012) 4999
7. Chen Y X, and Li H M, *J Mater Sci* **46** (2011) 957
8. Han-Guang F, and Kai-Hua H, *Modern Cast Iron* (2005) 32.
9. Guo C, and Kelly P M, *J Mater Sci* **39** (2004) 1109.
10. Sawada T, and Yanagitani A, *J Jpn Inst Metals* **73** (2009) 401.
11. Yi D W, Xing D J, Fu H G, Ma S Q, and Liu Z X, *Mater Technol* **26** (2013) 849.
12. Ma Y, Fu H G, Chen W, and Lei Y P, *Trans Mater Heat Treat* **36** (2015) 174.
13. Lv Z, Fu H G, Xing J D, Ma S Q, and Hu Y, *J Alloys Comps* **662** (2016) 54.
14. Ma Y, Fu H G, Yuan Y, Zhu L L, and Jiang L, *Foundry* **64** (2015) 950
15. Ju J, Fu H G, Fu D M, Wei S Z, Sang P, and Wu Z W, *Ironmak Steelmak* **45** (2018) 176
16. Kangzhen S, Shizhong W, and Zhen L, *J Henan Univ Sci Technol* **26** (2005) 4.
17. Haifeng L, Yaohui L, and Sirong Y, *Foundry* **49** (2000) 260.
18. Yue C X, Zhang L W, Liao S L, Pei J B, Gao H J, Jia Y W, and Lian X J, *Trans Mater Heat Treat* **29** (2008) 94.
19. Xiang P D, and Tang J X, *Hot Work Technol* 2004 21.
20. Xie J, Chen N X, Shen J, Teng L, and Seetharaman S, *Acta Mater* **53** (2005) 2727.
21. Fu H G, Song X D, Liu H M, Lei Y P, Cheng X L, and Xing J D, *Rare Metal Mater Eng* **39** (2010) 1125.